A Quantum-Limited CMOS-Sensor-Based High-Speed Imaging System for Time-Resolved X-Ray Scattering

Brian Rodricks[1], Boyd Fowler[1], Chiao Liu[1], John Lowes[1], Lucas J. Koerner[2], Mark W. Tate[2], Sol M. Gruner[2,3]
[1]Fairchild Imaging, 801 McCarthy Blvd, Milpitas, CA 95035
[2]Department of Physics, Cornell University, Ithaca, NY 14853
[3]Cornell High Energy Synchrotron Source, Ithaca, NY 14853

ABSTRACT

The field of ultrafast x-ray science is flourishing, driven by emerging synchrotron sources (e.g., time-slice storage rings, energy recovery linacs, free electron lasers) capable of fine time resolution. New hybrid x-ray detectors are under development in order to exploit these new capabilities.

This paper describes the development of a 2160 x 2560 CMOS image sensor (CIS) system with a 6.5 μm pitch optimized for time-resolved x-ray scattering studies. The system is single photon quantum limited from 8 keV to 20 keV. It has a wide dynamic range and can operate at 100 Hz full-frame and at higher frequencies using a region-of-interest (ROI) readout. Fundamental metrics of linearity, dynamic range, spatial resolution, conversion gain, sensitivity and Detective Quantum Efficiency are estimated. Experimental time-resolved data are also presented.

INTRODUCTION

The brilliance of x-ray beams has increased with the introduction of third-generation synchrotrons and will continue to grow as new linac-based sources, such as energy recovery linacs and x-ray free electron lasers, come on-line. These bright x-ray beams would allow many x-ray experiments, previously only considered for studying static structures, to probe dynamics of materials if sufficiently fast x-ray detectors are developed. X-ray area detectors based on CCDs that measure optical light from an x-ray stopping phosphor (indirect detection) have improved the speed and quality of x-ray image acquisition [1]. Yet, the serial nature of CCD readout constrains their temporal resolution, frequently requiring mechanical x-ray shutters, and data throughput. By contrast, the flexibility of the readout paradigms available to CMOS image sensors allows for finer temporal resolution, via electrical shuttering, as well as higher data throughput. Hybrid detectors (pixel array detectors) electrically couple a thick depleted x-ray stopping layer (direct detection) to a custom designed CMOS readout chip [2,3,4,5]. Hybrid pixel detectors have advanced time-resolved x-ray science in the fields of radiographic imaging of optically dense fluid sprays, powder diffraction of transient phase transformations, and fine-phi slicing crystallographic data collection [6,7,4], whetting community appetite for time-resolved x-ray experiments on myriad systems. Hybrid pixel detectors to date have relatively large pixels (c.a. 50 μm or larger), forcing multiple tiled repeats of a chip for a large format detector.

Hard X-Ray, Gamma-Ray, and Neutron Detector Physics XI, edited by Ralph B. James, Larry A. Franks, Arnold Burger,
Proc. of SPIE Vol. 7449, 74490Y · © 2009 SPIE · CCC code: 0277-786X/09/$18 · doi: 10.1117/12.828329

Another approach for high throughput and time-resolved x-ray imaging is configuration of scientific CMOS imagers [8], which now have noise levels comparable to CCD devices, for indirect x-ray detection. For example, a scientific CMOS imager coupled to a high-spatial resolution transparent luminescent screen would increase the data throughput and allow finer temporal resolution in x-ray microtomography [9,10]. Here we present characterization of a fast, high-format scientific CMOS imager with low noise and high data throughput configured for indirect x-ray detection via a standard Gd_2O_2S:Tb (Gadox) phosphor and a 1:1 fiber-optic coupling.

The CMOS sensor is a 2160 x 2560 pixel array with a 6.5 um pixel pitch. The details of the sensor development are given elsewhere[11]. The RMS electronic read-noise of the sensor is < 2e- at 30 frames/second (fps). Each column has two amplifiers, one with low-gain the other with high-gain. Each amplifier output drives an ADC. The results from the two converters are combined to provide a dynamic range greater than 16000:1. The quantum efficiency of the sensor at 550 nm is about 60%. The sensor has programmable region of interest readout that can increase the frame-rate from a maximum of 105 fps for a full-frame read to 1760 fps for a 128x128 region of interest.

X-RAY CAMERA

An x-ray camera was fabricated with a 2 mm fiber-optic faceplate glued to the CMOS sensor followed by a Gd_2O_2S:Tb phosphor (Gadox) screen. The Gadox screen was deposited on aluminized mylar to optimize light collection efficiency with a thickness optimized for 8 keV x-rays. This sandwich structure has two glue layers (Gadox to fiber optics and fiber optics to CMOS chip) that are thicker than the pixel pitch, thereby considerably reducing the spatial resolution. Figure 1 is a photograph of the sandwich structure.

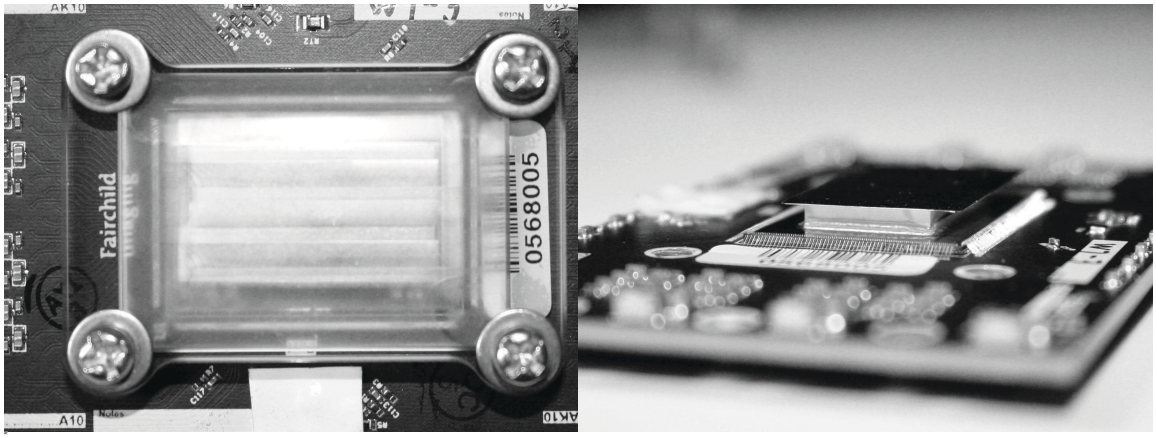

Fig. 1 Photograph of CMOS sensor glued to fiber-optic faceplate and scintillator. Left is top view and right is side profile.

SYSTEM ANALYSIS

The system was analyzed for dark-noise, photo-response and linearity, spatial resolution using the modulation transfer function (MTF) method, noise power spectrum (NPS), and detective quantum efficiency (DQE). Cu Kα x-radiation from a small tube source was

used to measure the fundamental metrics. The incident flux at a distance of 1 m from the source was measured to be 1 x-ray photon/pixel/sec using a Bicron NaI scintillation detector and a counter. The conversion gain of the CMOS sensor was estimated to be 2.5 digital counts/e^-.

The system was not cooled and had an operating temperature of 45° C. At this temperature the dark current was significant and needed to be accounted for in the analysis. In order to estimate the noise from the dark current, a series of dark images were collected with integration times from 20 ms to 5 s. Seventy images were captured at each integration time to estimate the variance. The mean variance of all pixels, after accounting for outliers (pixels with values $>\pm 5\sigma$), was estimated for each integration time and is displayed in Figure 2. The read-noise is the square-root of the variance at zero integration time and is estimated at 2 e^-/pixel.

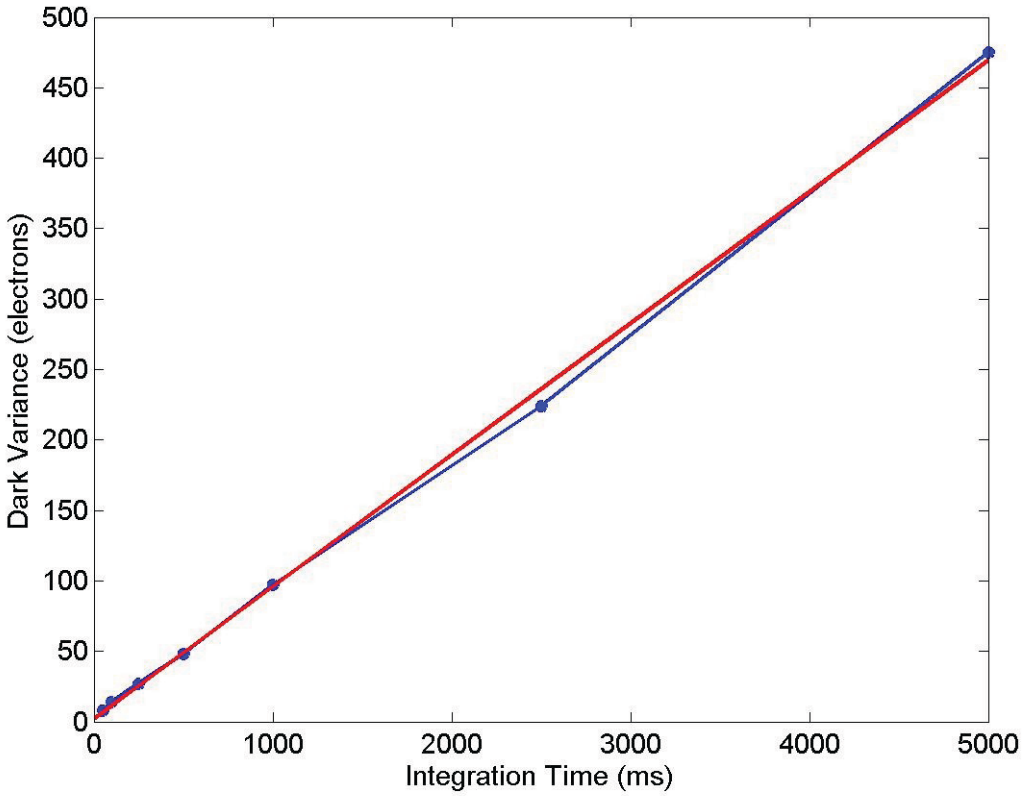

Fig. 2 Dark signal variance versus integration time.

In addition to measuring pixel fluctuations, the NPS was also measured using the dark acquisitions. For the NPS, two images at the same integration time were subtracted from each other to correct for dark signal non-uniformity (DSNU). A region of interest (ROI) of 512x512 pixels was used to measure the NPS. The NPS showed no spatial frequency dependence, a white spectrum, such that the average NPS value was the same as the statistically estimated variance. This indicated that there was no charge sharing between pixels during dark acquisitions.

With the x-ray source enabled, a series of x-ray images were captured with exposure times from 20 ms to 5000 ms. The average signal after dark subtraction was measured using a 100x100 pixel region of interest.

Figure 3 shows the photo-response of the imaging system to 8 keV x-radiation. The incident photon flux was ~1 x-ray photon/pixel/sec. The photo-response was measured at 26 e^-/x-ray photon.

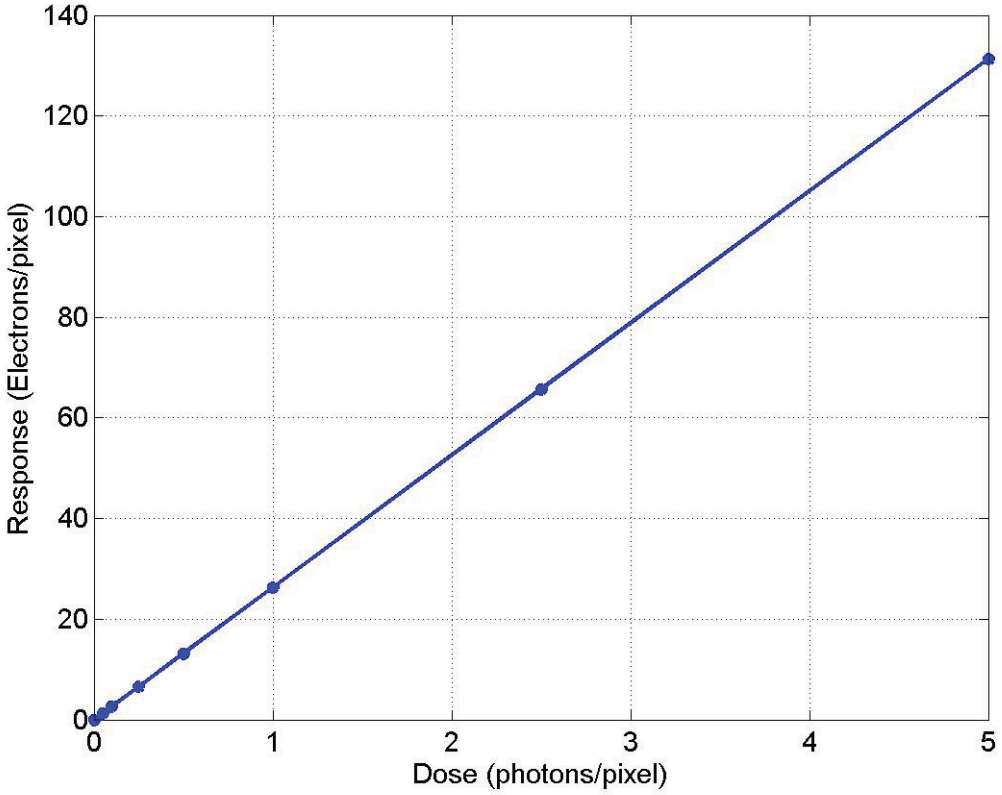

Fig. 3 Photo-response and linearity of the imaging system to 8 keV x-ray photons

The excellent correlation to a straight-line fit indicates a linear response for the imaging system.

The modulation transfer function quantifies the spatial resolution by evaluating the signal transfer through the imaging system as a function of spatial frequency. The MTF was measured using an edge inclined with respect to the detector's axis following the method prescribed by ISO 12233 [12].

Figure 4 is an image of the knife-edge and the resulting MTF. The Nyquist limit for the pixel pitch of 6.5 μm is approximately 77 lp/mm. The measured MTF falls to 50% at 3.2 lp/mm and 10% at 9.1 lp/mm [check these numbers] The large discrepancy between the limit set by the pixel-pitch and the measured MTF is largely attributable to the spreading

of the optical signal in the phosphor and the thickness of the glue lines. Each of the two glue lines are estimated to be about 20 μm in thickness.

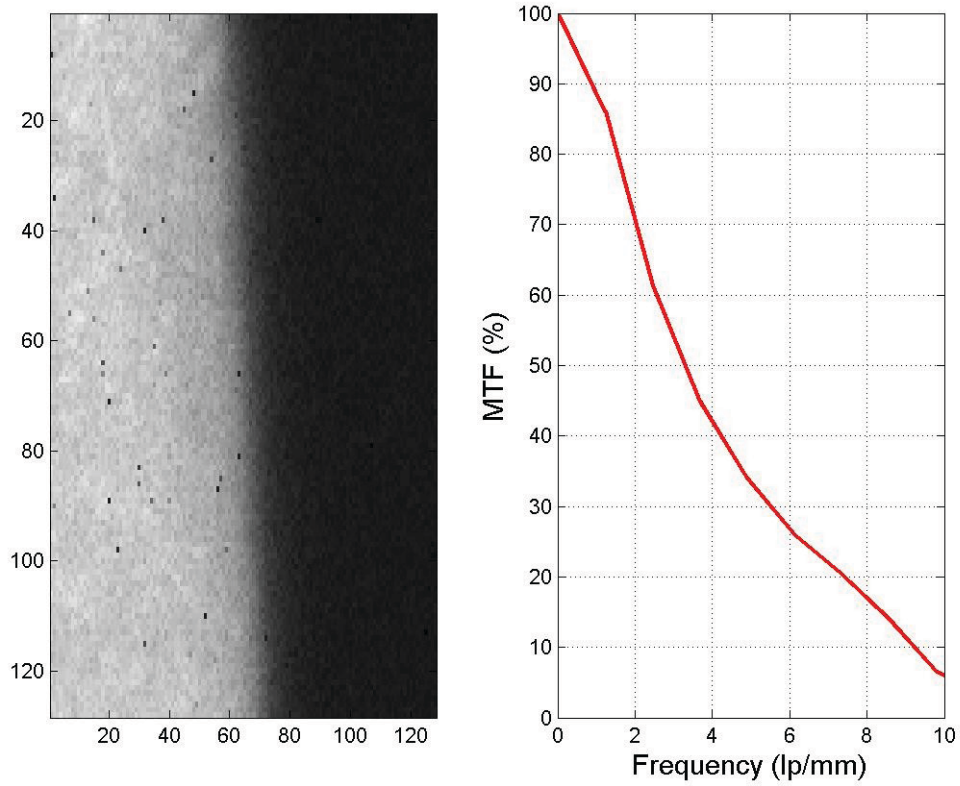

Fig. 4 The image of the knife-edge (left) and the measured MTF (right).

The image of the knife-edge is quite blurry, which is reflected in the MTF measurements. The MTF would be significantly improved by placing the phosphor-screen in direct contact with the CMOS sensor, or by having thinner glue layers.

The Detective Quantum Efficiency is a measure of how photons are utilized by the imaging system. Unlike the signal-to-noise-ratio, which increases in proportion to the signal, the DQE is invariant with signal once photon shot noise is the dominant noise source in the system. DQE is defined as

$$DQE = \frac{\left(s/\sigma\right)^2_{out}}{\left(s/\sigma\right)^2_{in}},$$

where s is the signal and σ is the noise.

Blurring of the signal from the spread of secondary optical photons induces correlations between pixels and reduces the noise measured by the detector with respect to input poisson fluctuations. Calculation of the input dose from the measured noise (photon transfer techniques) would produce an erroneous DQE. A technique developed by Gruner et. al.[13] evaluates the DQE associated with the measurement of the intensity of an x-ray spot. This procedure evaluates the detector's reproducibility of making a measurement common in x-ray science and also removes complications that arise from the input noise reduction caused by the point-spread-function.

The DQE was measured using a flat x-ray field occulted by a 51 μm thick tungsten mask with 75 μm diameter holes arranged on a square-grid with 1 mm spacing. For this measurement a copper anode x-ray tube was biased at 25 kV and 0.6 mA providing a flux of ~15 photons/pix/s. The x-rays/spot was varied from 1.6 to 2.4 $x10^3$ photons by adjusting the exposure time of the detector. After background subtraction, intensity correction, and row-fixed-pattern correction the intensity of 40 spots was found by integration of a circular region with radius of 15 pixels (609 pixels) from the calculated spot centroid and subtraction of the per-pixel background level found outside of the spots in an annulus with radii spanning 40-70 pixels from the spot centroid. To correct for fixed differences in hole-size inherent to the mask, variances of spot-intensity are calculated from pair-wise differences of the same mask-spot measured with the detector translated 500 μm between images. Translations in the pair-wise differences ensure that detector calibrations are evaluated. The variance of the differences and mean signal measured in the spots was calculated and averaged over 16 image pairs.

DQE(ω) for an imaging system can also be expressed as

$$DQE \;\alpha\; \frac{mtf(\omega)^2 \,/\, nps(\omega)}{\left(s/\sigma\right)^2_{in}},$$

where $mtf(\omega)^2/nps(\omega)$ is the $(s/\sigma)^2$ transferred through the imaging system.

The noise power spectrum also avoids the erroneous variance estimation from statistical analysis. The NPS close to zero frequency, which excludes nearby pixel correlations, shows the true variance of the input signal. At higher frequencies the NPS levels off and is reduced below incident poisson statistics by a factor dependent on the MTF and ultimately constrained by the poisson statistics of the secondary optical photons [15]. Although the NPS drops at high-frequencies, it does not result in higher DQE values because the MTF also drops at higher frequencies.

Figure 5 is a plot of the NPS as a function of frequency for varying incident photon fluxes.

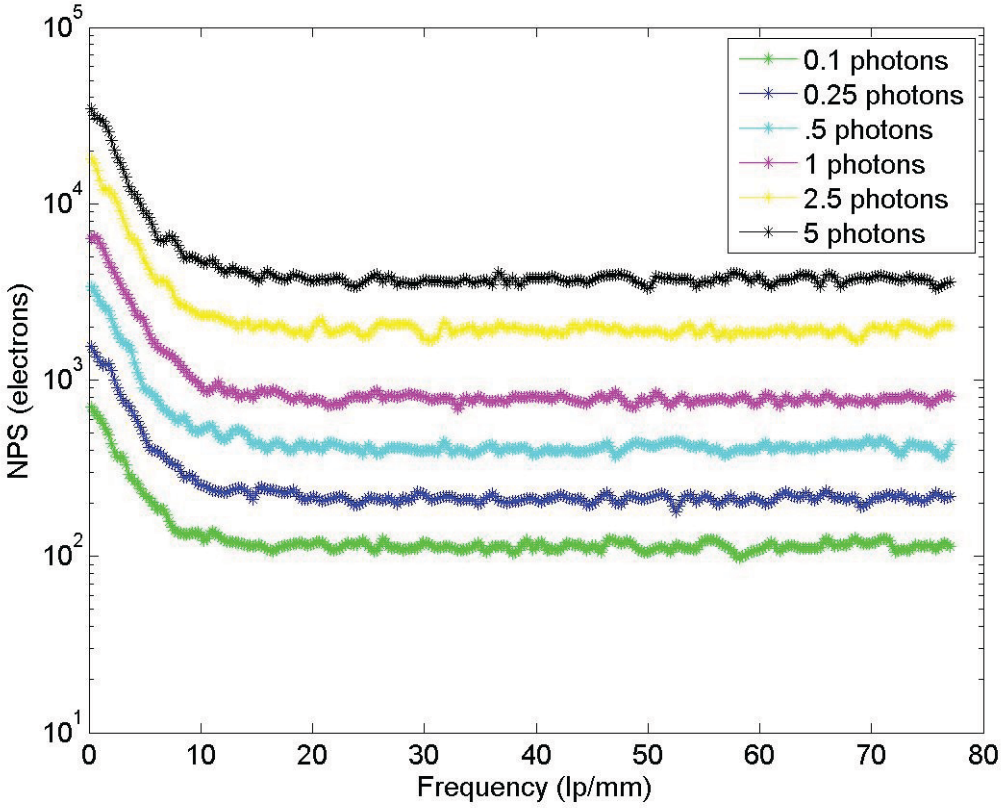

Fig. 5 The NPS as a function of frequency for a series of incident x-ray doses.

As expected, the NPS increases with increasing photon flux. Interestingly, the smoothing of the noise is clearly visible at all exposure levels.

Figure 6 is a plot of DQE. The left plot is the frequency dependent DQE measured at six incident dose levels. The right plot is the DQE evaluated from spot-mask measurements plotted versus average number of x-rays per spot.

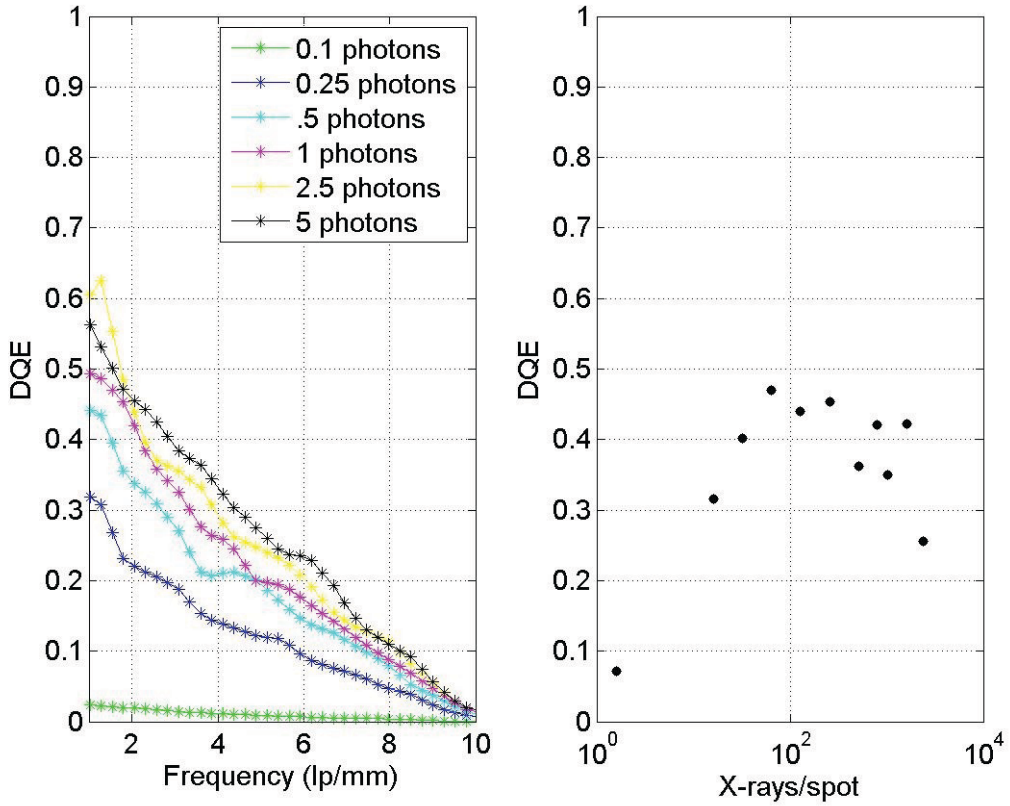

Fig. 6 The DQE as a function of incident flux. The left plot shows the frequency dependent DQE while the right plot shows the DQE versus dose for 75 µm spot llumination.

The frequency dependent DQE does not change significantly from 1 photon/pixel/sec to 5 photons/pixel/second indicating quantum-limited performance.

With regards to the pin-hole method of measuring DQE, the noise versus dose is considered to contain three distinct regions of dominate sources. At low dose the read-noise of the detector dominates the noise. At intermediate dose the quantum-efficiency and stochastic nature of the phosphor output dominate the noise. Finally, at high levels of dose systematic fixed pattern noise due to imperfect calibrations limit the accuracy. A model for the noise dependence upon dose is given as

$$\sigma^2 = A^2 + \frac{N_{x-ray}}{B} + (\mathrm{C\ x\ N}_{x-ray})^2 \text{ [14].}$$

For these measurements the read-noise in the integration spot was found to be 3.7 x-rays. The DQE at low-doses compares favorably to a high-efficiency fiber-optic

coupled CCD [13] with a 2.6:1 fiber-optic reduction ratio. This is a consequence of the low pixel read-noise of the CMOS imager and the higher number of electrons per x-ray with a 1:1 fiber-optic reduction ratio than a de-magnifying fiber-optic taper.

The x-ray camera can capture images at 100 frames/second with an exposure time of about 10 ms/frame. A rotating copper blade with a hole in it was placed in front of the camera and allowed to spin while images are captured. Figure 7 is a series of x-ray images captured at 100 fps. Notice the location of the copper mask changes from frame to frame.

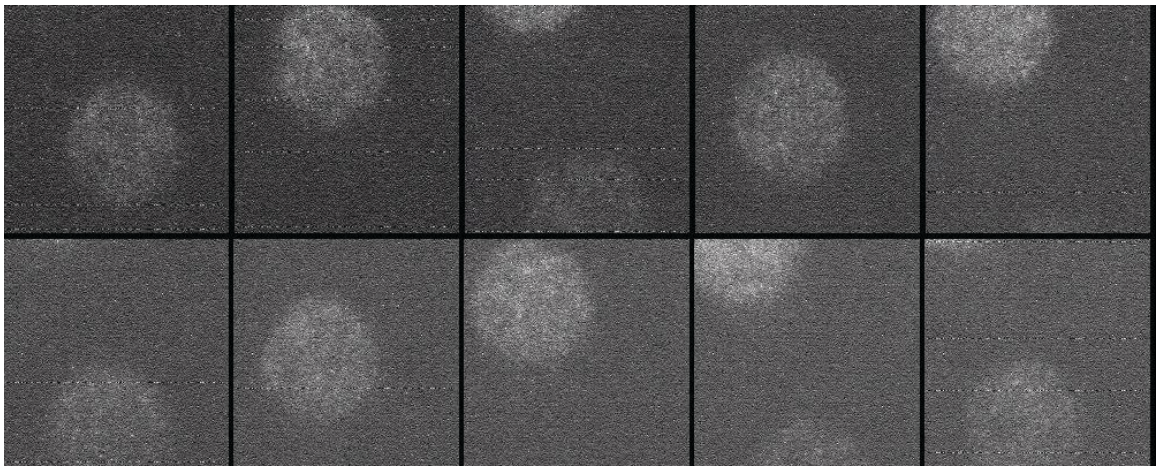

Fig. 7 A series on images taken approximately 10 ms apart. The circle is a hole in a Cu target.

SUMMARY

A scientific CMOS-based x-ray camera was evaluated using low x-ray photon flux of 1 photon/pixel/second. The read noise in the system was measured to be 2 e-. The system has an x-ray sensitivity of 26 electrons/8 keV x-ray photon. The MTF was limited to 10 lp/mm due to the glue line thickness. The DQE was measured to be about 40-45% around zero frequency and was limited by the quantum efficiency of the phosphor screen.

ACKNOWLEDGEMENTS

We would like to thank Dr. Shung Chieh and Colin Earle for supporting this scientific research. We would also like to thank Kumar Joshi for making the various flavors of x-ray sensors using combinations of FOPs and scintillators. We would also like to thank Sherwin Williams for help with the x-ray experiments and Lorna Schut for reviewing the manuscript. Time-resolved detector work in SMG's lab is supported by the DOE-BER grant DEFG-02-97ER62443 and by the Keck Foundation.

REFERENCES

[1] Sol M. Gruner, Mark W. Tate, and Eric F. Eikenberry, "Charge-coupled device area x-ray detectors," *Review of Scientific Instruments* 73, no. 8 (2002): 2815-2842.

[2] G. Rossi et al., "Tests of a prototype pixel array detector for microsecond time-resolved X-ray diffraction," *Journal of Synchrotron Radiation* 6, no. 6 (11, 1999): 1096-1105.

[3] L. J. Koerner, H.T. Philipp, M.S. Hromalik, M.W. Tate, S. M. Gruner, "X-ray tests of a Pixel Array Detector for coherent x-ray imaging at the Linac Coherent Light Source," *Journal of Instrumentation* 4, no. 03 (2009): P03001.

[4] Ch. Broennimann et al., "The PILATUS 1M detector," *Journal of Synchrotron Radiation* 13, no. 2 (2, 2006): 120-130.

[5] X. Llopart et al., "Medipix2: A 64-k pixel readout chip with 55-μm square elements working in single photon counting mode," *IEEE Transactions on Nuclear Science* 49 (October 1, 2002): 2279-2283.

[6] Wenyi Cai et al., "Quantitative analysis of highly transient fuel sprays by time-resolved x-radiography," *Applied Physics Letters* 83, no. 8 (2003): 1671-1673.

[7] Jonathan C. Trenkle et al., "Phase transformations during rapid heating of Al/Ni multilayer foils," *Applied Physics Letters* 93, no. 8 (2008): 081903-3.

[8] http://www.scmos.com/files/low/scmos_white_paper_2mb.pdf

[9] Andreas Koch et al., "X-ray imaging with submicrometer resolution employing transparent luminescent screens," *Journal of the Optical Society of America A* 15, no. 7 (July 1, 1998): 1940-1951.

[10] Y. J. Wang et al., "Quantitative x-ray phase-contrast imaging of air-assisted water sprays with high Weber numbers," *Applied Physics Letters* 89, no. 15 (October 9, 2006): 151913-3.

[11] Paul Vu, Boyd Fowler *et. al*. in preparation.

[12] http://webstore.ansi.org/RecordDetail.aspx?sku=ISO+12233%3a2000&source=google&adgroup=iso3&keyword=iso%2012233&gclid=CIe7hcuExZwCFR0SagodLicloA

[13] M. W. Tate et al., "A Large-Format High-Resolution Area X-ray Detector Based on a Fiber-Optically Bonded Charge-Coupled Device (CCD)," *Journal of Applied Crystallography* 28, no. 2 (4, 1995): 196-205.

[14] Mark W. Tate, Darol Chamberlain, and Sol M. Gruner, “Area x-ray detector based on a lens-coupled charge-coupled device,” *Review of Scientific Instruments* 76, no. 8 (2005): 081301-10.
[15] Jean-Pierre Moy, “Signal-to-noise ratio and spatial resolution in x-ray electronic imagers: Is the MTF a relevant parameter?,” *Medical Physics* 27, no. 1 (January, 2000): 86-93.